Received: 3 December 2022 | Revised: 27 February 2023 | Accepted: 15 March 2023

DOI: 10.1002/hbm.26291

RESEARCH ARTICLE

WILEY

# Altered large-scale dynamic connectivity patterns in Alzheimer's disease and mild cognitive impairment patients: A machine learning study

Rixing Jing[1] | Pindong Chen[2,3] | Yongbin Wei[4] | Juanning Si[1] | Yuying Zhou[5] | Dawei Wang[6] | Chengyuan Song[7] | Hongwei Yang[8] | Zengqiang Zhang[9] | Hongxiang Yao[10] | Xiaopeng Kang[2,3] | Lingzhong Fan[2] | Tong Han[11] | Wen Qin[12] | Bo Zhou[13] | Tianzi Jiang[2,3] | Jie Lu[8] | Ying Han[14,15,16] | Xi Zhang[13] | Bing Liu[17] | Chunshui Yu[12] | Pan Wang[5] | Yong Liu[2,3,4] | for the Alzheimer's Disease Neuroimaging Initiative

[1]School of Instrument Science and Opto-Electronics Engineering, Beijing Information Science and Technology University, Beijing, China

[2]Brainnetome Center & National Laboratory of Pattern Recognition, Institute of Automation, Chinese Academy of Sciences, Beijing, China

[3]School of Artificial Intelligence, University of Chinese Academy of Sciences, Beijing, China

[4]School of Artificial Intelligence, Beijing University of Posts and Telecommunications, Beijing, China

[5]Department of Neurology, Tianjin Huanhu Hospital, Tianjin University, Tianjin, China

[6]Department of Radiology, Qilu Hospital of Shandong University, Ji'nan, China

[7]Department of Neurology, Qilu Hospital of Shandong University, Ji'nan, China

[8]Department of Radiology, Xuanwu Hospital of Capital Medical University, Beijing, China

[9]Branch of Chinese PLA General Hospital, Sanya, China

[10]Department of Radiology, the Second Medical Centre, National Clinical Research Centre for Geriatric Diseases, Chinese PLA General Hospital, Beijing, China

[11]Department of Radiology, Tianjin Huanhu Hospital, Tianjin, China

[12]Department of Radiology, Tianjin Medical University General Hospital, Tianjin, China

[13]Department of Neurology, the Second Medical Centre, National Clinical Research Centre for Geriatric Diseases, Chinese PLA General Hospital, Beijing, China

[14]Department of Neurology, Xuanwu Hospital of Capital Medical University, Beijing, China

[15]Beijing Institute of Geriatrics, Beijing, China

[16]National Clinical Research Center for Geriatric Disorders, Beijing, China

[17]State Key Laboratory of Cognition Neuroscience & Learning, Beijing Normal University, Beijing, China

**Correspondence**
Pan Wang, Department of Neurology, Tianjin Huanhu Hospital, Tianjin University, Tianjin 300300, China.
Email: wpaofeier@163.com

## Abstract

Alzheimer's disease (AD) is a common neurodegeneration disease associated with substantial disruptions in the brain network. However, most studies investigated

Rixing Jing and Pindong Chen contributed equally to this study.

Data used in the preparation of this article were obtained from the Alzheimer's Disease Neuroimaging Initiative (ADNI) database (adni.loni.usc.edu). Therefore, the investigators within the ADNI contributed to the design and implementation of ADNI and/or provided data but did not participate in the analysis or writing of this report. A complete listing of the ADNI investigators is available at http://adni.loni.usc.edu/wp-content/uploads/how_to_apply/ADNI_Acknowledgement_List.pdf.

Yong Liu, School of Artificial Intelligence, Beijing University of Posts and Telecommunications, Beijing 100876, China.
Email: yongliu@bupt.edu.cn

**Funding information**
Beijing Natural Science Foundation, Grant/Award Numbers: 4214080, 7214299; Beijing Natural Science Funds for Distinguished Young Scholars, Grant/Award Number: JQ20036; Fundamental Research Funds for the Central Universities, Grant/Award Number: 2021XD-A03; National Natural Science Foundation of China, Grant/Award Numbers: 61633018, 81400890, 81471120, 81571062, 81871438, 81901101, 82172018; R&D Program of Beijing Municipal Education Commission, Grant/Award Number: KM202011232008; Tianjin Health Research Project, Grant/Award Number: TJWJ2022MS0321; National Institutes of Health, Grant/Award Numbers: W81XWH-12-2-0012, U01 AG024904; Department of Defense; National Institute on Aging; National Institute of Biomedical Imaging and Bioengineering; AbbVie; Alzheimer's Association; Alzheimer's Drug Discovery Foundation; Araclon Biotech; BioClinica, Inc.; Biogen; Bristol-Myers Squibb Company; CereSpir, Inc.; Cogstate; Eisai Inc.; Elan Pharmaceuticals, Inc.; Eli Lilly and Company; EuroImmun; F. Hoffmann-La Roche Ltd; Genentech, Inc.; Fujirebio; GE Healthcare; IXICO Ltd.; Janssen Alzheimer Immunotherapy Research & Development, LLC; Johnson & Johnson Pharmaceutical Research & Development, LLC; Lumosity; Lundbeck; Merck & Co., Inc.; Meso Scale Diagnostics, LLC; NeuroRx Research; Neurotrack Technologies; Novartis Pharmaceuticals Corporation; Pfizer Inc.; Piramal Imaging; Servier; Takeda Pharmaceutical Company; Transition Therapeutics; Canadian Institutes of Health Research

static resting-state functional connections, while the alteration of dynamic functional connectivity in AD remains largely unknown. This study used group independent component analysis and the sliding-window method to estimate the subject-specific dynamic connectivity states in 1704 individuals from three data sets. Informative inherent states were identified by the multivariate pattern classification method, and classifiers were built to distinguish ADs from normal controls (NCs) and to classify mild cognitive impairment (MCI) patients with informative inherent states similar to ADs or not. In addition, MCI subgroups with heterogeneous functional states were examined in the context of different cognition decline trajectories. Five informative states were identified by feature selection, mainly involving functional connectivity belonging to the default mode network and working memory network. The classifiers discriminating AD and NC achieved the mean area under the receiver operating characteristic curve of 0.87 with leave-one-site-out cross-validation. Alterations in connectivity strength, fluctuation, and inter-synchronization were found in AD and MCIs. Moreover, individuals with MCI were clustered into two subgroups, which had different degrees of atrophy and different trajectories of cognition decline progression. The present study uncovered the alteration of dynamic functional connectivity in AD and highlighted that the dynamic states could be powerful features to discriminate patients from NCs. Furthermore, it demonstrated that these states help to identify MCIs with faster cognition decline and might contribute to the early prevention of AD.

**KEYWORDS**
Alzheimer's disease, classification, dynamic connectivity, functional network

## 1 | INTRODUCTION

Alzheimer's disease (AD) is a common neurodegeneration disease associated with substantial disruptions in brain function (Braak & Braak, 1991; Scheltens et al., 2021). Extensive studies using functional magnetic resonance imaging (fMRI) have also suggested AD to be a disconnection syndrome (Delbeuck et al., 2007) with disrupted large-scale functional networks (Dai & He, 2014; Dennis & Thompson, 2014; Liu et al., 2014; Wang et al., 2013). Altered functional connectivity can reflect disease-specific damages (Seeley et al., 2009) and is associated with the amyloid β-protein (Aβ) burden in patients (Hahn et al., 2019). Mild cognitive impairment (MCI) is suggested to be an intermediate state between normal aging and dementia, which is considered a high-risk state for AD.

Previous studies have identified impairments in functional connectivity in multiple functional networks in AD, including the default mode network (DMN), the salience network, and the executive control network, and those altered functional activities might contribute to the disease diagnosis (Dai & He, 2014). In contrast to the commonly used stationary functional connectivity, emerging studies have started to investigate dynamic functional connectivity that provides a new perspective in the observation of dynamic activities and the understanding of the intrinsic organization of the brain (Agosta et al., 2012). The clinical relevance of dynamic functional connectivity and its potential utility as biomarkers have been reported in clinical studies in AD (Filippi et al., 2017), with abnormal dynamic functional connectivity mainly found in frontal and temporal cortices and associated with cognitive performances in AD (Gu et al., 2020). However, the small sample size and primary methods of those studies restricted the reliability and generalization. The understanding of the dynamic alteration and its potential diagnosis contribution in AD remains poorly studied.

Dynamic functional connectivity analysis usually uses the sliding time window method to compute dynamic functional connectivity (Allen et al., 2014). Clustering and decomposition methods were utilized to investigate the state of functional brain activity (Hutchison

et al., 2013; Preti et al., 2017), including K-means (Allen et al., 2014), principal component analysis (Leonardi et al., 2013), and independent component analysis (ICA) (Du et al., 2017; Miller et al., 2016; Yaesoubi et al., 2015). However, most studies only compared the group-level dynamic states between groups and ignored individual states and time-varying concentrations (Du et al., 2017). Notably, AD is a disorder that shows heterogeneity in clinical profile, pathology, and functional network (Chen et al., 2022; Lam et al., 2013), so the group-level dynamic functional connectivity might not capture the individual variability. Therefore, it is of essential importance to investigate the dynamic changes of functional activity more precisely by considering individual variability.

The primary aim of our study is to investigate the changes in dynamic time-varying characteristics by considering individual variability in AD and MCI. For this purpose, we used the group information guided ICA (GIG-ICA), an ICA framework for fMRI data analysis, to estimate the subject-specific inherent connectivity states individually based on dynamic functional connectivity patterns. GIG-ICA can adapt to the heterogeneity by capturing states at both group-level and subject-level and was widely applied to estimate subject-specific networks in psychiatric disorders (Jing et al., 2019; Jing et al., 2020; Salman et al., 2019). Then, a multivariate pattern classification technique was adopted to identify informative inherent states and built support vector machine (SVM) classifiers to distinguish ADs from normal controls (NCs). Finally, SVM classifiers based on AD and NC were used to group individuals with MCI. We investigate the dynamic features, cognition, gray matter volume, and cognition decline across MCI sub-groups (Figure 1).

## 2 | MATERIALS AND METHODS

### 2.1 | Participants

In this study, resting-state fMRI scans were acquired in 1704 individuals from three data sets. Data set 1 (young normal, YN) included 343 individuals with normal cognition. Data set 2 included 257 healthy NCs individuals, 257 MCI patients, and 295 AD patients from Multi-Center Alzheimer Disease Imaging Consortium Dataset (MCAD), including seven sites. Data set 3 included 259 NC, 184 subjects with MCI, and 109 AD patients from the Alzheimer's Disease Neuroimaging Initiative (ADNI) (www.adni.loni.usc.edu) database, which were used to investigate the longitudinal changes of MCI. The demographic, clinical information details, and ethics information are shown in Tables 1 and S1. Additional information about the ADNI data set was found at http://adni.loni.usc.edu/wp-content/uploads/how_to_apply/ADNI_Acknowledgement_List.pdf.

### 2.2 | Image acquisition and preprocessing

This section briefly overviews the MRI acquisition, preprocessing, and quality control with further details in the Supporting Information and our previous studies (Chen et al., 2022; Du et al., 2022; Jin, Wang, et al., 2020; J. Li et al., 2019; Qu et al., 2021). In Data set 1, individuals were scanned on one 3.0 T MRI scanner to obtain resting-state functional images (Tao et al., 2015). In Data set 2, individuals were scanned on one of seven different 3.0 T MRI scanners to obtain T1-weighted images and resting-state functional images (Chen et al., 2022; Qu et al., 2021), and the corresponding MRI acquisition protocols are described in Table S2. In Data set 3, individuals were scanned on a variety of 3.0 T scanners using standardized protocols at each site and resting-state functional images were included in the present study (http://adni.loni.usc.edu/methods/mri-tool/mri-acquisition/).

All the fMRI scans from three data sets were preprocessed using the Brainnetome Toolkit (http://brant.brainnetome.org) (Xu et al., 2018). The detailed information is described in our previous study (Jin, Wang, et al., 2020) and includes the following steps: (1) slice timing correction; (2) realignment to the first volume; (3) spatial normalization to MNI space at 2 mm × 2 mm × 2 mm; (4) regression of nuisance signals, including linear trends, six motion parameters, and their first-order differences, and signals representing white matter and cerebrospinal fluid; and (5) temporal bandpass filtering (0.01–0.08 Hz) to reduce high-frequency noise. Subsequently, any voxel for which the mean absolute deviation in the fMRI signal was less than 0.05 and any area that did not have an fMRI signal recorded from one or more participants was excluded. This resulted in a set of 263 regions of the Brainnetome Atlas (Fan et al., 2016) after quality control and this set was used in all further analyses (Jin, Wang, et al., 2020). The structural MRI images were preprocessed using the standard steps in the CAT12 toolbox (http://dbm.neuro.uni-jena.de/cat/, r1450), and the regional gray matter volume of each brain region was extracted using the Brainnetome Atlas (Fan et al., 2016).

### 2.3 | Identification of dynamic functional connectivity patterns

For each individual, we computed whole-brain time-varying functional connectivity matrices between all pairs of regions of the Brainnetome Atlas using a sliding time window method (window length = 60 s) as dynamic functional patterns (Allen et al., 2014). Connectivity strength (i.e., correlation coefficients) was transformed using Fisher's $z$ transformation. GIG-ICA was applied to the intra-group individuals' dynamic connectivity patterns to extract the subject-specific independent components as inherent connectivity states (ICSs) and the time-varying coefficients of each ICS (Du et al., 2017). The number of ICS was empirically determined to be 50.

In particular, NCs from Data set 1 were used to compute the group-level independent components by analyzing the window-direction concatenated dynamic connectivity patterns in an unbiased setting (detailed method can be found in the Supporting Information and elsewhere in our previous studies [Jing et al., 2020; Jing et al., 2019]). Then these components were used as guidance information to correspondingly back-reconstruct the subject-specific ICSs of the remaining participants from Data sets 2 and 3 using GIG-ICA. These ICSs were inter-individual variables and were similar within

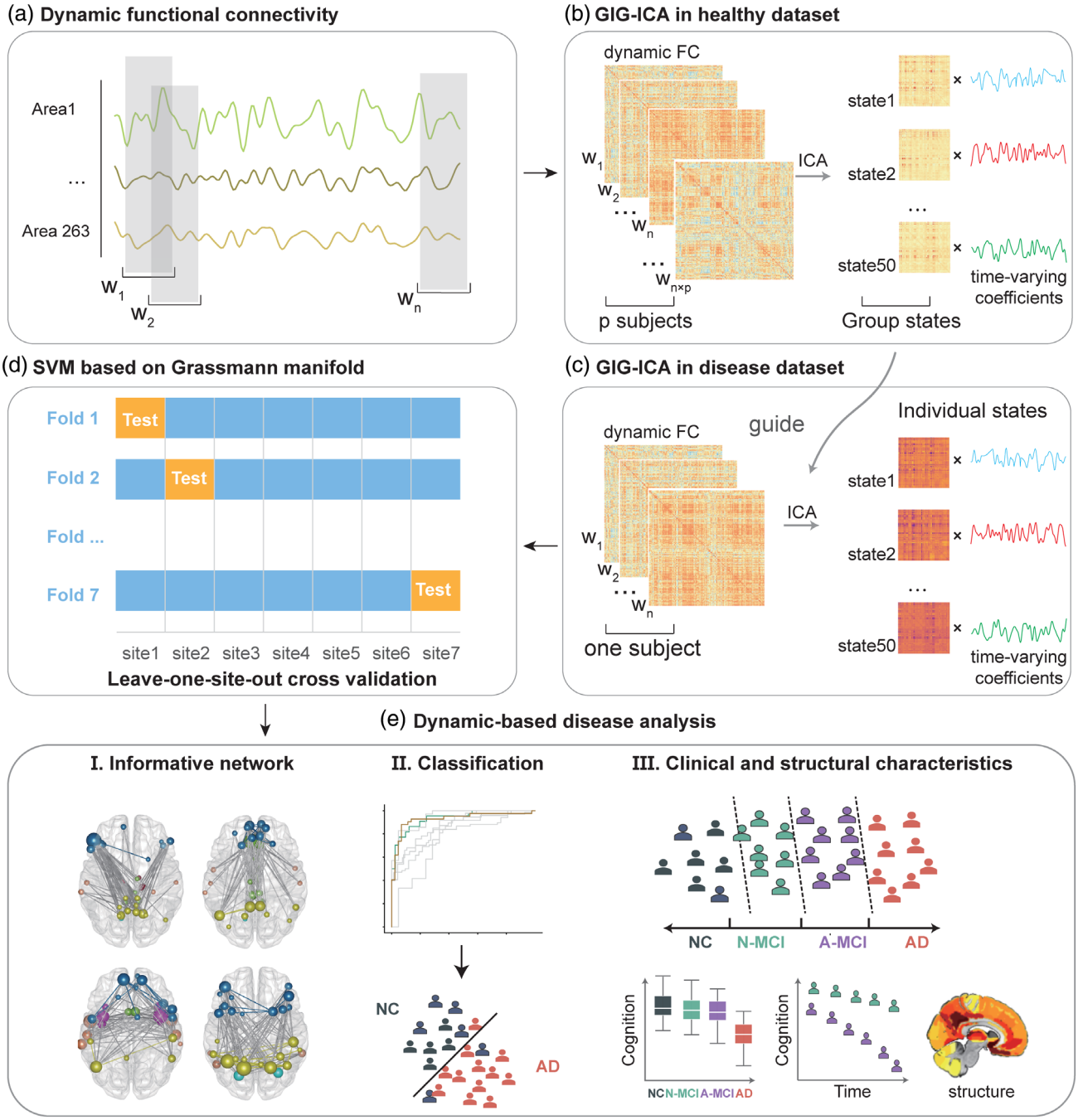


**FIGURE 1** Schematic of the dynamic functional connectivity analysis pipeline. (a) Acquisition of dynamic functional connectivity from fMRI. (b) The young normal sample from the Data set 1 was used to compute the group-level independent states, and then (c) these states were used as guidance information to calculate the subject-specific states of the remaining participants from two disease data sets (Data sets 2 and 3) using GIG-ICA. (d) A leave-one-site-out cross-validation procedure was used to identify the informative inherent states by using a simplified forward selection technique based on a support vector machine (SVM) model. (e) Abnormal dynamic characteristics of informative states were investigated (I) and classification was performed based on informative states between AD and NC (II). The individuals with MCI were divided into two subgroups based on their SVM scores, and the statistical analysis was performed on the clinical and structural characteristics between groups (III). AD, Alzheimer's disease; fMRI, functional magnetic resonance imaging; MCI, mild cognitive impairment; NC, normal control.

each group. Finally, the dynamic functional connectivity of each subject was characterized by 50 ICSs and their corresponding time-varying weight coefficients. Notably, for each subject, all states estimated in ICA back-reconstruction were normalized by removing the mean value of dynamic connectivity patterns.

## 2.4 | Supervised feature selection to identify the informative inherent connectivity states

To investigate the importance of ICSs and avoid feature redundancy, we selected ICSs using a simplified forward selection technique based

**TABLE 1** Demographic characteristics per data set.

| Data set | Group | *n* | Gender (M/F) | *p* | Age | *p* | MMSE | *p* |
|---|---|---|---|---|---|---|---|---|
| Data set 1 (YN) | NC | 343 | 187/156 | – | 31.18 ± 11.39 | – | – | – |
| Data set 2 (MCAD) | NC | 257 | 104/153 | .66[a] | 66.93 ± 6.83 | .01[b] | 28.52 ± 1.64 | <.001[b] |
| | MCI | 257 | 114/143 | | 68.56 ± 8.91 | | 25.14 ± 3.39 | |
| | AD | 295 | 123/172 | | 68.89 ± 8.27 | | 16.56 ± 6.02 | |
| Data set 3 (ADNI) | NC | 259 | 115/144 | .54[a] | 71.5 ± 6.0 | .07[b] | 29.0 ± 1.1 | <.001[b] |
| | MCI | 184 | 102/82 | | 72.0 ± 7.8 | | 28.0 ± 1.7 | |
| | AD | 109 | 59/50 | | 73.3 ± 7.2 | | 22.6 ± 3.6 | |

Abbreviations: AD, Alzheimer's disease; MCAD, Multi-Center Alzheimer Disease Imaging Consortium Dataset; MCI, mild cognitive impairment; MMSE, Mini-Mental State Examination; NC, normal control; YN, young normal.

[a]$\chi 2$ test.

[b]One-way analysis of variance.

on an SVM model. The kernel SVM model was determined by the similarity measures defined as the Riemannian distance on the Grassmann manifold between samples computed based on their ICSs (Fan et al., 2011; P. Li et al., 2017).

Specifically, we utilized a leave-one-site-out cross-validation procedure to identify the critical ICSs for AD classification in Data set 2. At each cross-validation time, one site was the testing set, with the other six sites as the training set. On each training set, 10-fold cross-validation was applied to build aggregated SVM classifier and to select an optimal combination of ICSs with the forward component selection algorithm (Figure 2a) (Jing et al., 2019, 2020). The forward selection algorithm built a classifier upon each ICS, and all ICSs were sorted by the area under the receiver operating characteristic curve (AUC; first rank) and classification accuracy (second rank) numerically from the largest to the smallest. Then, by combining the first $k$ ($k = 1, 2, \ldots, 50$) ordered ICSs sequentially, 50 classifiers were built and the classification performance of those was obtained. Finally, the combination of ICSs with the overall best classification performance was chosen as the most discriminative ICSs. A nested 10-fold cross-validation was used to optimize the parameters of classifiers. We could get the selection frequency of each ICS after the whole 70 times forward selections. Finally, informative ICSs of AD were identified as those selected with higher frequency.

## 2.5 | Functional annotation for informative ICSs based on Neurosynth

To investigate the potential cognitive functions of informative ICSs, we used the online platform Neurosynth (https://neurosynth.org/), which includes meta-analytic brain maps on a large amount of human functional neuroimaging studies (Yarkoni et al., 2011). First, we calculated the strength of each region (sum of the weighted edges linked to each region) for each informative ICS, and the negative weight of nodes was set to zeros. Then, the region-based data were mapped to volume images that were used as input to identify region-associated cognitive terms through the Neurosynth "decoder" function. Finally, the mental terms with correlations >.1 were visualized on a word-cloud plot, with sizes scaled according to their correlations with the corresponding meta-analytic maps, excluding anatomical terms (Sha et al., 2022).

## 2.6 | Classification between AD and NC based on informative ICSs

The multivariate pattern classification method using the leave-one-site-out cross-validation procedure based on the selected informative ICSs was applied to individuals in the seven sites in Data set 2. The classification approach based on the selected informative ICSs was repeatedly applied to individuals in seven training and testing loops. In each site-specific testing loop, the 10-fold cross-validation model yielded 10 SVM classifiers for distinguishing AD patients from NCs. We set the median value of classification scores of these nested 10-fold cross-validation classifiers as the classification score for each subject in the test site, with a positive classification score to indicate AD or a negative value to indicate NC. Nonparametric permutation tests were used to estimate the statistical significance of the classification performance. The null distribution of the AUC was estimated for all site-specific SVM models by performing 100 leave-one-site-out cross-validation permutation tests with subject class labels randomly permuted, resulting in 700 AUCs of permutation tests.

We adopted a certainty measure ($\max(\frac{n_p}{n}, \frac{n_n}{n})$ to evaluate the classification reliability for each subject based on the aggregated classifiers, where $n_p$ and $n_n$ are the number of positive or negative classification scores, respectively, and $n$ is the total number of classifiers [here, $n = 10$ in Data set 2]; Jing et al., 2019). A higher value indicated higher classification reliability and vice versa. We excluded subjects with lower classification certainty (<0.8) in post hoc analyses. To validate the generalization of the informative ICSs selected in Data set 2, we also independently performed the classification based on the informative ICSs in Data set 3. We conducted 50 times random-hold-out validation with 90 AD and 90 NC in each iteration to keep the sample size balanced.

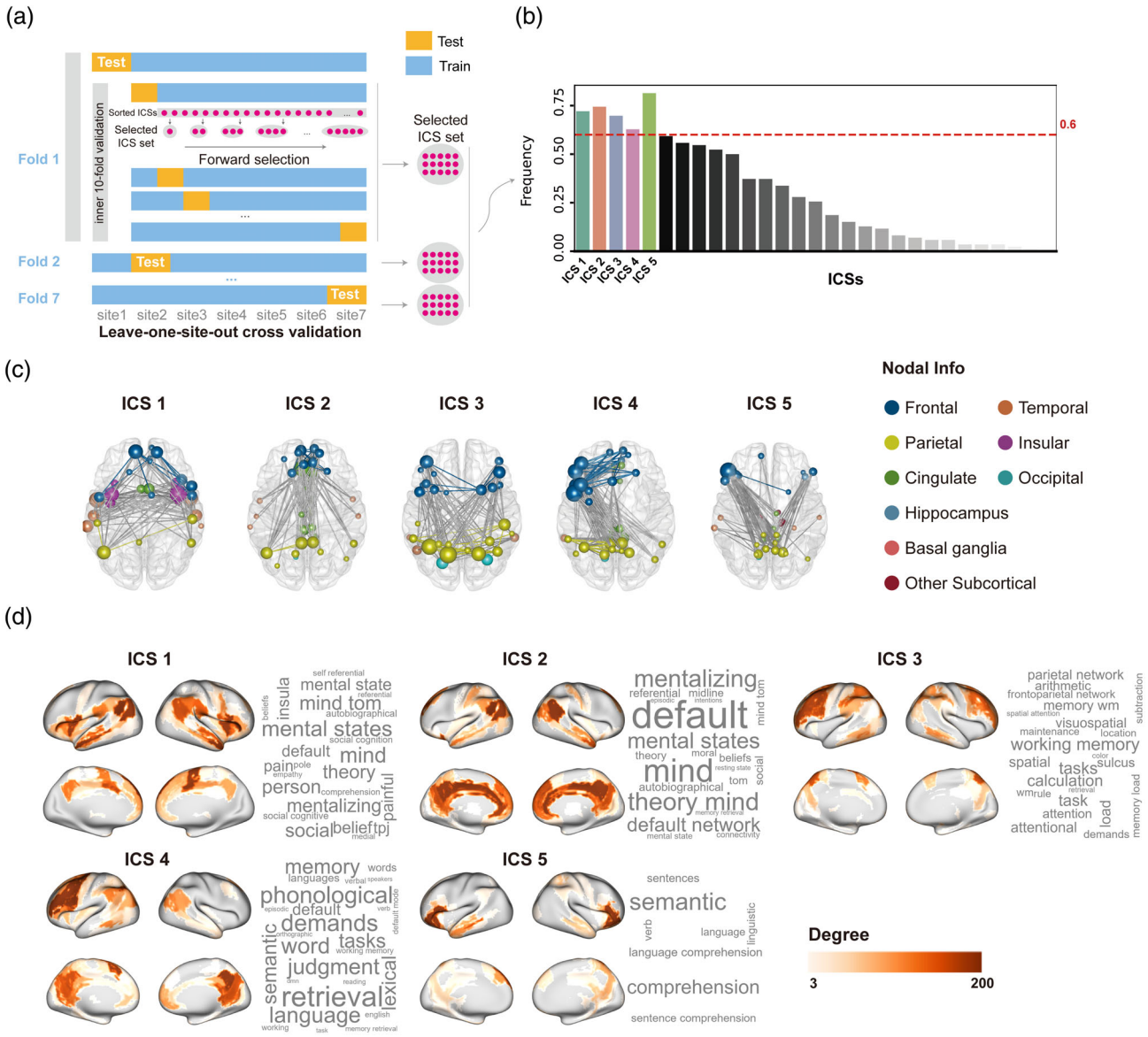


**FIGURE 2** Informative ICSs and functional annotation. (a) Schematic of the cross-validation scheme to select informative ICSs for each of the seven scanners. (b) The selected frequency of all the ICSs. The ICSs with the top 5 selected frequencies were informative ICSs. (c) Functional connectivity weight of informative ICSs derived from the feature selection. Node size represents the degree of each region. (d) The brain map weighted by the network degree and functional annotation of informative ICSs. Word cloud figures showed the functional items ($r > .1$) derived from a meta-analysis on Neurosynth. ICS, inherent connectivity state.

## 2.7 | Subgrouping MCI based on informative ICSs

The site-specific classifiers were applied to the ICSs of MCIs, so each MCI was given 10 individual classification scores. The median of the 10 individual classification scores was used as a robust measure to characterize the affinity of each MCI to AD. Positive classification scores reflected an AD-specific functional pattern, and negative scores indicated an NC-specific way. So, MCIs with classification scores >0 were assigned to the AD-specific subgroup (A-MCI), and those with classification scores <0 were assigned to the NC-specific subgroup (N-MCI). We also adopted a certainty measure to evaluate the classification reliability for each subject based on the aggregated classifiers. We excluded subjects with lower classification certainty (<0.8) in post hoc analyses.

Moreover, to assess whether the dynamic measures could reveal different cognitive impairment progressions, we used MCI patients from Data set 3 and divided them into two subgroups based on the fitted model in Data set 3. Linear mixed models were used to evaluate longitudinal cognition decline over time. The month from baseline (the visit session scanned fMRI), subgroup, and their interaction were included as fixed effects ($p < .05$). Subject intercepts and slopes were modeled as random effects. Age and sex were also considered as covariates.

### 2.8 | Correlation with clinical measures

A general linear model was used to investigate the correlations between the classification scores and MMSE in groups with age, sex, and site covariates to explore the relationship between the classification output and clinical measures in Data set 2.

### 2.9 | Comparisons of brain intrinsic, structural, and clinical characteristics

The functional connectivity strength in the informative ICSs was compared between any two groups using pseudo-two-sample *t* tests (SnPM13; http://warwick.ac.uk/snpm; $p = .05$, permutation tests $n = 5000$, age, sex, and site as covariates). We also investigated the group differences of fluctuation coefficients and synchronization coefficients of informative ICSs by a two-sample two-sided *t* test to explore if functional states' changes were associated with dynamic alterations (age, sex, and site as covariates). The fluctuation coefficient was the average change of the frame-wise variation of each informative ICS's time-varying weight coefficients. The synchronization coefficient was calculated by partial correlation analysis between all pairs of informative ICSs based on time-varying weight coefficients.

We also investigated the group differences between NC, MCI subgroups, and AD in clinical and structural characteristics by using a two-sample *t* test in a similar setting. The MMSE score was compared between groups with age, sex, and site as covariates. The difference in regional gray matter volume between the two MCI subgroups was investigated by using a two-sample *t* test with age, sex, site, and total intracranial volume as covariates ($p < .05$, FDR corrected across all regional volume tests performed).

### 2.10 | Replication experiment on the Power's 264 functional ROIs

To further validate the robustness of the method and the main results of the present study, we replicated the experiment using the same scans and similar procedures. The only difference was the calculation of the dynamic functional connectivity matrices based on Power's 264 functional ROIs (Power et al., 2011) instead of the Brainnetome Atlas. In addition, the confusion matrix of the subgroups' results from two experiments was used to quantify the robustness of the results.

## 3 | RESULTS

### 3.1 | Informative ICSs in AD identified by pattern classification

The top five informative ICSs (Figure 2b, frequency > 0.6) were conserved after the feature selection (Figure 2a). The associated functional connectivity of each informative ICS is shown in Figure 2c. ICS1 involved functional connectivity in the middle temporal gyrus, inferior frontal gyrus, and precuneus. ICS2 included the bilateral superior temporal gyrus, the precuneus, the cingulate gyrus, and the medial prefrontal lobe, which connected the middle prefrontal lobe with the anterior cingulate gyrus and parietal lobe. Most of the functional connections of ICS3 were involved in the bilateral dorsolateral prefrontal lobe and the precuneus. ICS4 had functional connections that connected the left dorsolateral prefrontal lobe and inferior parietal lobule. ICS5 mainly includes the functional connectivities between the inferior frontal gyrus and superior parietal lobule.

### 3.2 | Functional annotation for informative ICS

Based on the meta-analysis on Neurosynth, the most prominently shared functional annotation for informative ICSs that showed alterations in AD were the "Default mode network (DMN)" (Figure 2d and Table S3). Notably, each network also had additional cognitive annotations. Briefly, ICS1 involved cortical regions associated with mental states, mind, and social behavior. The functional annotation of ICS2 showed the relevance of the mind and the DMN. Areas with ICS3 linked to the dorsal lateral prefrontal cortex were associated with working memory and attention tasks. ICS4 was more relevant to language tasks. Finally, ICS5 involved regions related to semantics, comprehension, language comprehension, and sentences.

### 3.3 | Classification between AD and NC

The average accuracy of the classifiers built upon the informative ICSs with leave-one-site-out cross-validation was 79% (sensitivity 85% and specificity 70%), with a mean AUC of 0.87 (highest AUC of 0.95) in Data set 2 (Figure 3a). The classification results of each test site were summarized in Table S4. Nonparametric permutation tests showed that the classification results were statistically significant ($p < .01$, 100 permutations), as indicated by the histogram of permuted AUC shown in Figure 3a. It is worth noting that 96% of the individuals had high classification certainty (>0.8), and those with lower confidence were excluded in post hoc analysis. We also applied the classifiers that optimally separated ADs and NCs to the states of MCIs in Data set 2. As a result, the classification scores of MCI and AD were negatively correlated with their MMSE ($r = -.53$, $p < .001$) (Figure 3b). Moreover, the performance is relatively lower in Data set 3 (AUC = 0.75, ACC = 0.68, specificity = 0.66, and sensitivity = 0.75) than in Data set 2.

### 3.4 | Quantify MCIs with probable conversion to AD

Individuals with MCI were classified using the models fitted in AD discrimination. According to the classification scores, MCI subjects showed heterogeneity. We divided them into two subgroups: subjects

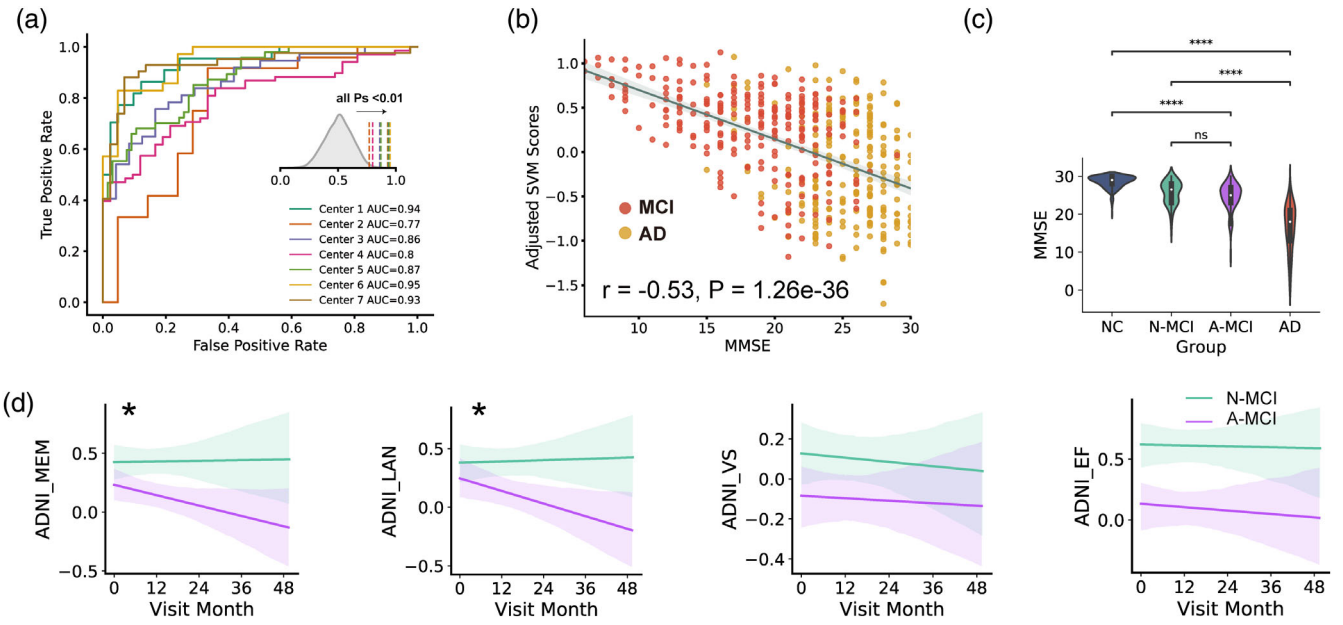


**FIGURE 3** Classification between AD and NC based on informative ICSs. (a) The receiver operating characteristic curves (ROCs) and area under ROCs (AUC) of inter-site cross-validations. (b) Correlation between the SVM scores and MMSE. (c) The comparison of MMSE between groups. (d) The cognition declines over the follow-up of the two subgroups of MCI. (*: $p < .05$, ****: $p < .00001$). AD, Alzheimer's disease; ICS, inherent connectivity state; MCI, mild cognitive impairment; MMSE, Mini-Mental State Examination; SVM, support vector machine.

had AD-specific states (classification scores > 0) as probable AD converters (A-MCI), and 126 subjects had NC-specific states (classification scores < 0) as probable non-converter (N-MCI). Notably, 95% of the patients with MCI had high classification certainty (>0.8), and those with lower confidence were excluded in post hoc analysis. There was no significant difference in MMSE between the A-MCI and N-MCI, while the MMSE scores of A-MCI were relatively lower than that of NC and the MMSE scores of N-MCI were relatively higher than that of AD (*ps* <.001; Figure 3c).

In Data set 3, 91 MCI were divided into A-MCI and 93 into N-MCI based on the model fitted in AD. About 131 (71%) patients with MCI had high classification certainty (>0.8). The two subgroups of MCI had different cognition decline progressions (Figure 3d). A-MCI had a faster decline in composite measures for memory (ADNI-MEN) and language (ADNI-LAN) than N-MCI (All *ps* <.05). In contrast, the two groups had similar decline progression in composite measures for executive function (ADNI-EF) and visuospatial functioning (ADNI-VS; Table S6).

## 3.5 | Dynamic characteristics between groups

Pseudo-*t* tests were conducted to compare the functional connectivity of informative ICSs among AD, NC, A-MCI, and N-MCI groups (Figure 4a). Compared with NCs, ADs, and A-MCIs shared similar weaker connectivities in all informative ICSs, with ADs showing the largest alterations. Also, A-MCIs had weaker connectivities than N-MCIs, with a similar pattern as AD versus NC. The A-MCIs exhibited higher connectivities in ICS1, ICS4, and ICS5 (partial connections), while weaker connectivities in ICS2, ICS3, and ICS5 (partial connections) than in AD. In addition, the N-MCIs exhibited higher connectivities in ICS1, ICS2, ICS3 (partial connections), ICS4 (partial connections), and ICS5, with weaker ones in ICS3 (partial connections) and ICS4 (partial connections) than in NCs. The results delineated those abnormalities in the connectivity of the informative ICSs largely overlapped in AD and A-MCI, while N-MCI had a few abnormal alterations.

The dynamic characteristics of the brain states changed in varying degrees (Figure 4b,c). The fluctuating coefficients of AD and NC showed significant differences in ICS1 ($p = .023$), ICS2 ($p = .010$), and ICS4 ($p = .039$). Meanwhile, significant differences were found in ICS2 for N-MCI versus AD ($p = .022$), A-MCI versus NC ($p = .015$), and A-MCI versus N-MCI ($p = .026$). Moreover, the synchronization coefficient comparisons indicated that AD and A-MCI are associated with more alterations in inter-ICS synchronization. ICS1 shows the most synchronous changes. ICS 1–2 synchronization and ICS 1–3 synchronization showed a significant increase in AD versus NC, AD versus N-MCI, A-MCI versus NC, and A-MCI versus N-MCI (*ps* < .001). ICS 1–4 synchronization and ICS 1–5 synchronization showed a decrease in AD versus NC (*ps* < .01). The synchronization of other ICS also shows different degrees of difference between groups. ICS 2–4 synchronization and ICS 3–4 synchronization also showed a significant increase in AD versus NC, AD versus N-MCI, A-MCI versus NC, and A-MCI versus N-MCI (*ps* < .01). Besides, ICS 4–5 synchronization showed a decrease in AD vs. NC, AD vs. N-MCI, A-MCI vs. NC, and A-MCI vs. N-MCI (*ps* < .01). No significant difference was found across groups in synchronizations of ICS3 and ICS2, as well as ICS3 and ICS5. It should be noted that the A-MCI and AD showed similar alteration patterns, while N-MCI showed few alterations compared with NC.

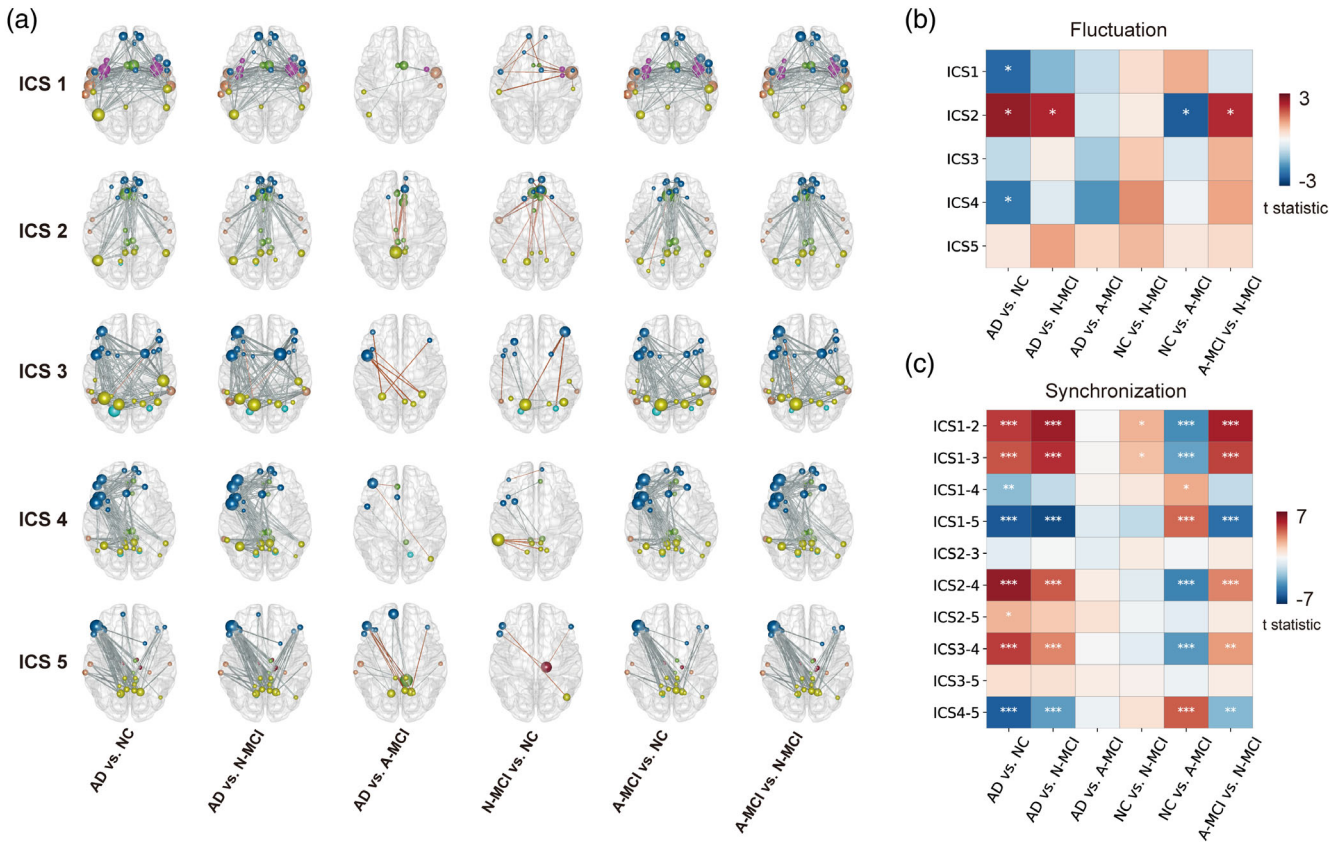


**FIGURE 4** Clinical and brain intrinsic characteristics comparisons. (a) The differences in functional connectivity of informative ICSs among AD, NC, A-MCI, and N-MCI groups. Red lines represent the increased connectivity and the gray ones represent the decreased connectivity. Node size represents the degree of each region. (b) Comparison of the fluctuation of informative ICSs between NC, N-MCI, A-MCI, and AD. (c) Comparisons on synchronization between informative ICSs in NC, N-MCI, A-MCI, and AD. (*: $p < .05$, **: $p < .01$, ***: $p < .001$). A-MCI, AD-specific subgroup; AD, Alzheimer's disease; ICS, inherent connectivity state; MCI, mild cognitive impairment; N-MCI, NC-specific subgroup; NC, normal control.

### 3.6 | Structural characteristics between groups

Compared to NC, patients with AD showed widespread atrophies in the whole brain, while the participants with A-MCI showed slighter atrophy in the cortex and dominant atrophy in the temporal lobe and hippocampus (Figure 5). The N-MCI showed rare atrophy in most areas of the cortex and slighter atrophy in the temporal lobe, cingulate gyrus, thalamus, hippocampus, and inferior parietal lobule. Notably, the A-MCI showed more atrophy in the hippocampus, anterior cingulate, temporal lobe, and thalamus than N-MCI. These results suggested that the dynamics reflected characteristics are associated with the structural changes in the AD spectrum.

### 3.7 | Replication experiment on the Power's 264 functional ROIs

Two ICSs were identified based on the Power's parcellation (Figure S2) and the model's classification accuracy was 75% (sensitivity 80% and specificity 65%) with an AUC of 0.82 in Data set 2 (Table S5). The individuals with MCI from the same sites were divided into two subgroups based on Power's 264 Atlas, and the confusion matrix of the subgroups' division between Power's 264 Atlas and the Human Brainnetome Atlas was shown in Figure S3. In two experiments, 76.4% of the individuals with MCI were identified as A-MCI twice and 77.7% were as N-MCI twice. The results verified that this approach was robust and obtained good division.

## 4 | DISCUSSION

The present study recovered abnormal dynamic functional states and their temporal properties in the AD spectrum by disease discrimination in a large multicenter data set. The five dynamic functional states not only had good features for discriminating AD and NC accurately (mean AUC = 0.87) but also showed alterations in functional connectivity strength, fluctuation, and inter-synchronization. More importantly, our results showed that changes in dynamic states began in the MCI stage with only subtle symptoms and could be used to reveal the different progression of MCI. These results highlight that the dynamic states can be a powerful feature in discriminating diseased patients from NCs and might contribute to identifying prognosis markers of MCI.

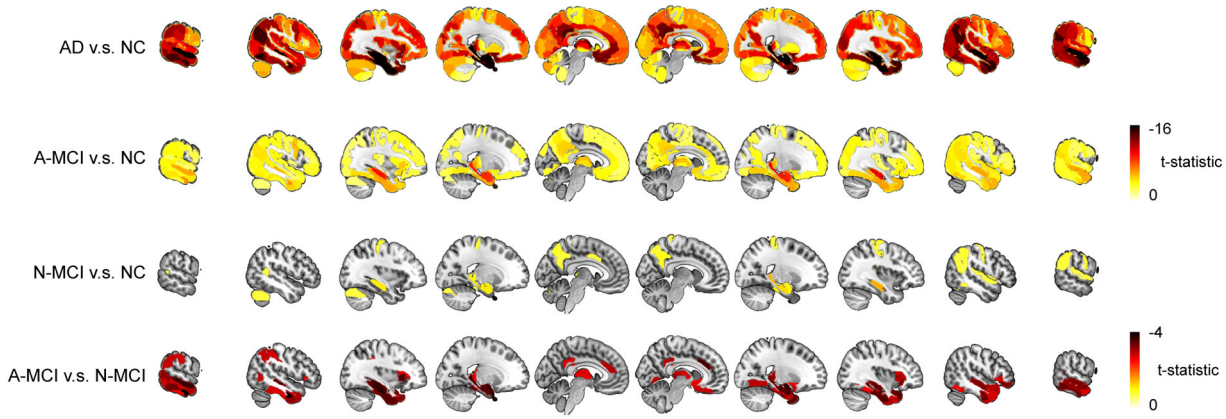


**FIGURE 5** Structural characteristics comparisons between groups. Regional gray matter volume was compared between groups using *t* test ($p_{FDR}$ <.05).

A novel multivariate classification framework was proposed by using optimized data-driven methods. Instead of obtaining group-level dynamics (Hutchison et al., 2013), we used GIG-ICA to extract personalized dynamics. Independent cross-site validation was also used for evaluating the machine learning model (Abraham et al., 2017). Compared with previous studies based on dynamic functional connectivity, higher accuracy and stability of classification were obtained (de Vos et al., 2018; Niu et al., 2019). More importantly, the classification performance could achieve the same level (mean AUC = 0.87) of multiple complex functional features (i.e., functional connectivity, the amplitude of local brain activity, functional connectivity strength and regional homogeneity, etc.; Jin, Wang, et al., 2020), with only the subject-specific dynamic functional connectivity, suggesting that abnormal dynamics could provide additional information for detecting AD (Deco & Corbetta, 2011). Furthermore, the replication results with an independent ADNI data set and second brain atlas strength showed that our findings were highly reproducible.

Previous studies showed that MCI and AD were associated with disruptions of functional networks, which were associated with memory, execution, visuospatial ability, and attention (Agosta et al., 2012; Badhwar et al., 2017; Chen et al., 2023; Dennis & Thompson, 2014; Eyler et al., 2019; Jones et al., 2016). The DMN is associated with various cognitive functions and is preferentially disrupted in AD (Dennis & Thompson, 2014; Eyler et al., 2019). Our results corroborated these findings, showing a dynamics disruption in the DMN in AD. Informative ICS2 showed a spatial pattern similar to DMN, and other Informative ICSs were involved in the DMN. In addition, disrupted functional brain networks are not only restricted to inner DMN (Agosta et al., 2012). Informative ICS1 involved functional connectivity between the DMN and the salience network. The salience network was especially associated with emotion and social behavior, contributing to the social–emotional function changes in AD (Zhou & Seeley, 2014). The frontoparietal network also showed connectivity disruptions in AD (Badhwar et al., 2017). The frontoparietal network and DMN interacted in Informative ICS3, demonstrating a link between working memory and attention tasks. Moreover, language function disrupted in AD showed an association with informative ICS4 and ICS5. The five functional networks derived from informative ICSs were a disentanglement of the complex disruption of functional systems in AD (Cohen, 2018). Our findings suggest the mutidomain cognition impairment in AD under large-scale functional network disruption might be due to the dynamics damage of multiple brain networks (Dai & He, 2014; Dennis & Thompson, 2014; Liu et al., 2014; Wang et al., 2013).

It is well-accepted that the brain is a complex system for information transmission. The brain networks were divided into dynamic states (ICSs) using GIG-ICA, and the integrative structure of intra- and inter-informative ICSs was uncovered simultaneously. Most of the strengths of functional connectivity decreased in the informative ICSs in AD, which is consistent with the disconnection mechanisms of AD (Dai & He, 2014). Notably, several synchronizations between ICSs increased. Segregated ICSs showed more synchronizations might indicate the functional specialization of brain networks disrupted in AD (Chan et al., 2014; Ewers et al., 2021; Liu et al., 2014). Moreover, altered brain dynamic functional states dwell time and complexity, such as DMN-associated states in MCI and AD, were supported by previous studies (Nunez et al., 2021; Sendi et al., 2021). Consistently, we observed the fluctuation of ICS1 and ICS4 decreased significantly in AD compared with NC. The fluctuation of ICS2 increased in AD compared with NC and N-MCI. ICS2 overlaps with the DMN; the larger fluctuation of it might cause disrupted activity and lower dwell time (Nunez et al., 2021; Sendi et al., 2021).

More importantly, the dynamic characteristics also revealed the different cognition declines of MCI. The more similar dynamic states to NC corresponded to a slower decline rate, which reminded us that the early changes of AD were associated with the dynamic state changes. The N-MCI and A-MCI did not have a significant difference in cognition in Data set 2, which might be due to the functional activity changes beyond the measurable pathology and followed neurodegeneration (Jones et al., 2016). The changes in dynamics in MCI were

more about synchronizations rather than fluctuation, reminding us that the early changes of AD might associate with inter-network synchronization. Several progression markers have been identified as predictive factors of the converter from MCI to AD (Jin, Zhou, et al., 2020). In this study, the association with cognition showed that dynamic functional patterns might be a valuable predictor of disease progression. Moreover, converging evidence suggests that individuals with MCI might belong to different subgroups with different risks (Young et al., 2018; Zhao et al., 2022). The A-MCI subjects with positive classification scores shared quite similar dynamic patterns (strength of the informative ICSs, fluctuations, and synchronizations) with AD patients, indicating a higher risk of converting. The structural change was also found between the two subgroups of MCI, indicating the classifiers built on the informative ICSs could be biomarkers for discovering brain structural alternation.

This study has several limitations. First, the group-level ICSs identified in Data set 1 guided the back-reconstruction of the subject-specific ICSs in the other two data sets. Using the independent data sets for group-level ICSs is beneficial to avoid looking twice at data sets in different steps of analysis. However, Data set 1 is a younger normal sample, while Data sets 2 and 3 are older disease samples. Although the demographic and clinical differences might bring some bias, replication analysis with the group-level ICSs derived from healthy individuals in Data set 2 showed a similar result, indicating our main findings to be not biased by the demographic differences (Supporting Information: Results S1). Second, acquisition scanning protocols differed across the studied sites should be noted. Instead of directly pooling data from all sites, we performed a leave-one-site-out cross-validation for pattern classification and applied the site-specific models to the corresponding subjects. Third, longitudinal data were unavailable in the in-house data set, so we used the participants with MCI from ADNI as an independent site for validation. Finally, the participants' cognitive function was only characterized by MMSE in MCAD. Other cognitive measures should be collected to facilitate a more comprehensive characterization of the brain function for further elucidating the differences between the A-MCI and N-MCI.

In conclusion, the present study using multisite data sets suggests that abnormal dynamic functional connectivity patterns identified by a multivariate classification method were informative for quantifying brain alternation in AD. The classification scores of the MCIs and ADs were associated with cognitive ability. The identified A-MCI individuals shared similar intrinsic brain patterns to the AD patients regarding functional connectivity strength, fluctuation, and inter-synchronization. These findings suggest that the dynamic states could reveal the different progression of MCI and may help to recognize high-risk MCI subjects early.

## ACKNOWLEDGMENTS

Data collection and sharing for this project were funded by the Alzheimer's Disease Neuroimaging Initiative (ADNI) (National Institutes of Health Grant U01 AG024904) and DOD ADNI (Department of Defense award number W81XWH-12-2-0012). ADNI is funded by the National Institute on Aging, the National Institute of Biomedical Imaging and Bioengineering, and through generous contributions from the following: AbbVie; Alzheimer's Association; Alzheimer's Drug Discovery Foundation; Araclon Biotech; BioClinica, Inc.; Biogen; Bristol-Myers Squibb Company; CereSpir, Inc.; Cogstate; Eisai Inc.; Elan Pharmaceuticals, Inc.; Eli Lilly and Company; EuroImmun; F. Hoffmann-La Roche Ltd and its affiliated company Genentech, Inc.; Fujirebio; GE Healthcare; IXICO Ltd.; Janssen Alzheimer Immunotherapy Research & Development, LLC; Johnson & Johnson Pharmaceutical Research & Development, LLC; Lumosity; Lundbeck; Merck & Co., Inc.; Meso Scale Diagnostics, LLC; NeuroRx Research; Neurotrack Technologies; Novartis Pharmaceuticals Corporation; Pfizer Inc.; Piramal Imaging; Servier; Takeda Pharmaceutical Company; and Transition Therapeutics. The Canadian Institutes of Health Research is providing funds to support ADNI clinical sites in Canada. Private sector contributions are facilitated by the Foundation for the National Institutes of Health (www.fnih.org). The grantee organization is the Northern California Institute for Research and Education, and the study is coordinated by the Alzheimer's Therapeutic Research Institute at the University of Southern California. ADNI data are disseminated by the Laboratory for Neuro Imaging at the University of Southern California. This work was partially supported by the Beijing Natural Science Foundation (Grant nos. 7214299 and 4214080), the Fundamental Research Funds for the Central Universities (Grant no. 2021XD-A03), the Beijing Natural Science Funds for Distinguished Young Scholars (Grant no. JQ20036), R&D Program of Beijing Municipal Education Commission (Grant no. KM202011232008), Tianjin Health Research Project (Grant no. TJWJ2022MS0321), and the National Natural Science Foundation of China (Grant nos. 81871438, 82172018, and 81901101). Data collection and sharing for this project were funded by the National Natural Science Foundation of China (Grant Nos. 61633018, 81571062, 81400890, and 81471120).

## CONFLICT OF INTEREST STATEMENT

The authors declare no conflict of interest.

## DATA AVAILABILITY STATEMENT

The data that support the findings of this study are available from the corresponding author upon reasonable request. All ADNI data are deposited in a publicly accessible repository and can be accessed at ADNI (http://adni.loni.usc.edu/). The code that was used can be obtained at GitHub (https://github.com/YongLiuLab)

## ORCID

*Rixing Jing* https://orcid.org/0000-0002-4123-0385
*Pindong Chen* https://orcid.org/0000-0003-4655-786X
*Wen Qin* https://orcid.org/0000-0002-9121-8296
*Tianzi Jiang* https://orcid.org/0000-0001-9531-291X
*Jie Lu* https://orcid.org/0000-0003-0425-3921
*Bing Liu* https://orcid.org/0000-0003-2029-5187
*Chunshui Yu* https://orcid.org/0000-0001-5648-5199
*Yong Liu* https://orcid.org/0000-0002-1862-3121

## REFERENCES


Abraham, A., Milham, M. P., Di Martino, A., Craddock, R. C., Samaras, D., Thirion, B., & Varoquaux, G. (2017). Deriving reproducible biomarkers from multi-site resting-state data: An autism-based example. *NeuroImage*, *147*, 736–745. https://doi.org/10.1016/j.neuroimage.2016.10.045

Agosta, F., Pievani, M., Geroldi, C., Copetti, M., Frisoni, G. B., & Filippi, M. (2012). Resting state fMRI in Alzheimer's disease: Beyond the default mode network. *Neurobiology of Aging*, *33*(8), 1564–1578. https://doi.org/10.1016/j.neurobiolaging.2011.06.007

Allen, E. A., Damaraju, E., Plis, S. M., Erhardt, E. B., Eichele, T., & Calhoun, V. D. (2014). Tracking whole-brain connectivity dynamics in the resting state. *Cerebral Cortex*, *24*(3), 663–676. https://doi.org/10.1093/cercor/bhs352

Badhwar, A., Tam, A., Dansereau, C., Orban, P., Hoffstaedter, F., & Bellec, P. (2017). Resting-state network dysfunction in Alzheimer's disease: A systematic review and meta-analysis. *Alzheimer's & Dementia*, *8*, 73–85. https://doi.org/10.1016/j.dadm.2017.03.007

Braak, H., & Braak, E. (1991). Neuropathological stageing of Alzheimer-related changes. *Acta Neuropathologica*, *82*(4), 239–259. https://doi.org/10.1007/BF00308809

Chan, M. Y., Park, D. C., Savalia, N. K., Petersen, S. E., & Wig, G. S. (2014). Decreased segregation of brain systems across the healthy adult lifespan. *Proceedings of the National Academy of Sciences of the United States of America*, *111*(46), E4997–E5006. https://doi.org/10.1073/pnas.1415122111

Chen, P., Yao, H., Tijms, B. M., Wang, P., Wang, D., Song, C., Yang, H., Zhang, Z., Zhao, K., Qu, Y., Kang, X., Du, K., Fan, L., Han, T., Yu, C., Zhang, X., Jiang, T., Zhou, Y., Lu, J., … Alzheimer's Disease Neuroimaging Initiative. (2022). Four distinct subtypes of Alzheimer's disease based on resting-state connectivity biomarkers. *Biological Psychiatry*, *93*(9), 759–769. https://doi.org/10.1016/j.biopsych.2022.06.019

Chen, P., Zhao, K., Zhang, H., Wei, Y., Wang, P., Wang, D., Song, C., Yang, H., Zhang, Z., Yao, H., Qu, Y., Kang, X., Du, K., Fan, L., Han, T., Yu, C., Zhou, B., Jiang, T., Zhou, Y., Lu, J., … Alzheimer's Disease Neuroimaging Initiative. (2023). Altered global signal topography in Alzheimer's disease. *eBioMedicine*, *89*, 104455. https://doi.org/10.1016/j.ebiom.2023.104455

Cohen, J. R. (2018). The behavioral and cognitive relevance of time-varying, dynamic changes in functional connectivity. *NeuroImage*, *180* (Pt B), 515–525. https://doi.org/10.1016/j.neuroimage.2017.09.036

Dai, Z., & He, Y. (2014). Disrupted structural and functional brain connectomes in mild cognitive impairment and Alzheimer's disease. *Neuroscience Bulletin*, *30*(2), 217–232. https://doi.org/10.1007/s12264-013-1421-0

de Vos, F., Koini, M., Schouten, T. M., Seiler, S., van der Grond, J., Lechner, A., Schmidt, R., de Rooij, M., & Rombouts, S. (2018). A comprehensive analysis of resting state fMRI measures to classify individual patients with Alzheimer's disease. *NeuroImage*, *167*, 62–72. https://doi.org/10.1016/j.neuroimage.2017.11.025

Deco, G., & Corbetta, M. (2011). The dynamical balance of the brain at rest. *The Neuroscientist*, *17*(1), 107–123. https://doi.org/10.1177/1073858409354384

Delbeuck, X., Collette, F., & Van der Linden, M. (2007). Is Alzheimer's disease a disconnection syndrome? Evidence from a crossmodal audio-visual illusory experiment. *Neuropsychologia*, *45*(14), 3315–3323. https://doi.org/10.1016/j.neuropsychologia.2007.05.001

Dennis, E. L., & Thompson, P. M. (2014). Functional brain connectivity using fMRI in aging and Alzheimer's disease. *Neuropsychology Review*, *24*(1), 49–62. https://doi.org/10.1007/s11065-014-9249-6

Du, K., Chen, P., Zhao, K., Qu, Y., Kang, X., Liu, Y., & Multi-center Alzheimer Disease Imaging Consortium. (2022). Impaired time-distance reconfiguration patterns in Alzheimer's disease: A dynamic functional connectivity study with 809 individuals from 7 sites. *BMC Bioinformatics*, *23*(Suppl 6), 280. https://doi.org/10.1186/s12859-022-04776-x

Du, Y., Pearlson, G. D., Lin, D., Sui, J., Chen, J., Salman, M., Tamminga, C. A., Ivleva, E. I., Sweeney, J. A., Keshavan, M. S., Clementz, B. A., Bustillo, J., & Calhoun, V. D. (2017). Identifying dynamic functional connectivity biomarkers using GIG-ICA: Application to schizophrenia, schizoaffective disorder, and psychotic bipolar disorder. *Human Brain Mapping*, *38*(5), 2683–2708. https://doi.org/10.1002/hbm.23553

Ewers, M., Luan, Y., Frontzkowski, L., Neitzel, J., Rubinski, A., Dichgans, M., Hassenstab, J., Gordon, B. A., Chhatwal, J. P., Levin, J., Schofield, P., Benzinger, T. L. S., Morris, J. C., Goate, A., Karch, C. M., Fagan, A. M., McDade, E., Allegri, R., Berman, S., … Alzheimer's Disease Neuroimaging Initiative and the Dominantly Inherited Alzheimer Network. (2021). Segregation of functional networks is associated with cognitive resilience in Alzheimer's disease. *Brain*, *144*(7), 2176–2185. https://doi.org/10.1093/brain/awab112

Eyler, L. T., Elman, J. A., Hatton, S. N., Gough, S., Mischel, A. K., Hagler, D. J., Franz, C. E., Docherty, A., Fennema-Notestine, C., Gillespie, N., Gustavson, D., Lyons, M. J., Neale, M. C., Panizzon, M. S., Dale, A. M., & Kremen, W. S. (2019). Resting state abnormalities of the default mode network in mild cognitive impairment: A systematic review and meta-analysis. *Journal of Alzheimer's Disease*, *70*(1), 107–120. https://doi.org/10.3233/JAD-180847

Fan, L., Li, H., Zhuo, J., Zhang, Y., Wang, J., Chen, L., Yang, Z., Chu, C., Xie, S., Laird, A. R., Fox, P. T., Eickhoff, S. B., Yu, C., & Jiang, T. (2016). The Human Brainnetome Atlas: A new brain atlas based on connectional architecture. *Cerebral Cortex*, *26*(8), 3508–3526. https://doi.org/10.1093/cercor/bhw157

Fan, Y., Liu, Y., Wu, H., Hao, Y., Liu, H., Liu, Z., & Jiang, T. (2011). Discriminant analysis of functional connectivity patterns on Grassmann manifold. *NeuroImage*, *56*(4), 2058–2067. https://doi.org/10.1016/j.neuroimage.2011.03.051

Filippi, M., Basaia, S., Canu, E., Imperiale, F., Meani, A., Caso, F., Magnani, G., Falautano, M., Comi, G., Falini, A., & Agosta, F. (2017). Brain network connectivity differs in early-onset neurodegenerative dementia. *Neurology*, *89*(17), 1764–1772. https://doi.org/10.1212/WNL.0000000000004577

Gu, Y., Lin, Y., Huang, L., Ma, J., Zhang, J., Xiao, Y., Dai, Z., & Alzheimer's Disease Neuroimaging Initiative. (2020). Abnormal dynamic functional connectivity in Alzheimer's disease. *CNS Neuroscience & Therapeutics*, *26*(9), 962–971. https://doi.org/10.1111/cns.13387

Hahn, A., Strandberg, T. O., Stomrud, E., Nilsson, M., van Westen, D., Palmqvist, S., Ossenkoppele, R., & Hansson, O. (2019). Association between earliest amyloid uptake and functional connectivity in cognitively unimpaired elderly. *Cerebral Cortex*, *29*(5), 2173–2182. https://doi.org/10.1093/cercor/bhz020

Hutchison, R. M., Womelsdorf, T., Allen, E. A., Bandettini, P. A., Calhoun, V. D., Corbetta, M., Della Penna, S., Duyn, J. H., Glover, G. H., Gonzalez-Castillo, J., Handwerker, D. A., Keilholz, S., Kiviniemi, V., Leopold, D. A., de Pasquale, F., Sporns, O., Walter, M., & Chang, C. (2013). Dynamic functional connectivity: Promise, issues, and interpretations. *NeuroImage*, *80*, 360–378. https://doi.org/10.1016/j.neuroimage.2013.05.079

Jin, D., Wang, P., Zalesky, A., Liu, B., Song, C., Wang, D., Xu, K., Yang, H., Zhang, Z., Yao, H., Zhou, B., Han, T., Zuo, N., Han, Y., Lu, J., Wang, Q., Yu, C., Zhang, X., Zhang, X., … Liu, Y. (2020). Grab-AD: Generalizability and reproducibility of altered brain activity and diagnostic classification in Alzheimer's disease. *Human Brain Mapping*, *41*(12), 3379–3391. https://doi.org/10.1002/hbm.25023

Jin, D., Zhou, B., Han, Y., Ren, J., Han, T., Liu, B., Lu, J., Song, C., Wang, P., Wang, D., Xu, J., Yang, Z., Yao, H., Yu, C., Zhao, K., Wintermark, M., Zuo, N., Zhang, X., Zhou, Y., … Liu, Y. (2020). Generalizable, reproducible, and neuroscientifically interpretable imaging biomarkers for Alzheimer's disease. *Advanced Science*, *7*(14), 2000675. https://doi.org/10.1002/advs.202000675

Jing, R., Han, Y., Cheng, H., Han, Y., Wang, K., Weintraub, D., & Fan, Y. (2020). Altered large-scale functional brain networks in neurological Wilson's disease. *Brain Imaging and Behavior*, *14*(5), 1445–1455. https://doi.org/10.1007/s11682-019-00066-y

Jing, R., Li, P., Ding, Z., Lin, X., Zhao, R., Shi, L., Yan, H., Liao, J., Zhuo, C., Lu, L., & Fan, Y. (2019). Machine learning identifies unaffected first-degree relatives with functional network patterns and cognitive impairment similar to those of schizophrenia patients. *Human Brain Mapping*, *40*(13), 3930–3939. https://doi.org/10.1002/hbm.24678

Jones, D. T., Knopman, D. S., Gunter, J. L., Graff-Radford, J., Vemuri, P., Boeve, B. F., Petersen, R. C., Weiner, M. W., Jack, C. R., Jr., & Alzheimer's Disease Neuroimaging Initiative. (2016). Cascading network failure across the Alzheimer's disease spectrum. *Brain*, *139*(Pt 2), 547–562. https://doi.org/10.1093/brain/awv338

Lam, B., Masellis, M., Freedman, M., Stuss, D. T., & Black, S. E. (2013). Clinical, imaging, and pathological heterogeneity of the Alzheimer's disease syndrome. *Alzheimer's Research & Therapy*, *5*(1), 1. https://doi.org/10.1186/alzrt155

Leonardi, N., Richiardi, J., Gschwind, M., Simioni, S., Annoni, J. M., Schluep, M., Vuilleumier, P., & Van De Ville, D. (2013). Principal components of functional connectivity: A new approach to study dynamic brain connectivity during rest. *NeuroImage*, *83*, 937–950. https://doi.org/10.1016/j.neuroimage.2013.07.019

Li, J., Jin, D., Li, A., Liu, B., Song, C., Wang, P., Wang, D., Xu, K., Yang, H., Yao, H., Zhou, B., Bejanin, A., Chetelat, G., Han, T., Lu, J., Wang, Q., Yu, C., Zhang, X., Zhou, Y., … Han, Y. (2019). ASAF: Altered spontaneous activity fingerprinting in Alzheimer's disease based on multisite fMRI. *Science Bulletin*, *64*(14), 998–1010. https://doi.org/10.1016/j.scib.2019.04.034

Li, P., Jing, R. X., Zhao, R. J., Ding, Z. B., Shi, L., Sun, H. Q., Lin, X., Fan, T. T., Dong, W. T., Fan, Y., & Lu, L. (2017). Electroconvulsive therapy-induced brain functional connectivity predicts therapeutic efficacy in patients with schizophrenia: A multivariate pattern recognition study. *NPJ Schizophrenia*, *3*, 21. https://doi.org/10.1038/s41537-017-0023-7

Liu, Y., Yu, C., Zhang, X., Liu, J., Duan, Y., Alexander-Bloch, A. F., Liu, B., Jiang, T., & Bullmore, E. (2014). Impaired long distance functional connectivity and weighted network architecture in Alzheimer's disease. *Cerebral Cortex*, *24*(6), 1422–1435. https://doi.org/10.1093/cercor/bhs410

Miller, R. L., Yaesoubi, M., Turner, J. A., Mathalon, D., Preda, A., Pearlson, G., Adali, T., & Calhoun, V. D. (2016). Higher dimensional meta-state analysis reveals reduced resting fMRI connectivity dynamism in schizophrenia patients. *PLoS One*, *11*(3), e0149849. https://doi.org/10.1371/journal.pone.0149849

Niu, H., Zhu, Z., Wang, M., Li, X., Yuan, Z., Sun, Y., & Han, Y. (2019). Abnormal dynamic functional connectivity and brain states in Alzheimer's diseases: Functional near-infrared spectroscopy study. *Neurophotonics*, *6*(2), 025010. https://doi.org/10.1117/1.NPh.6.2.025010

Nunez, P., Poza, J., Gomez, C., Rodriguez-Gonzalez, V., Hillebrand, A., Tewarie, P., Tola-Arribas, M. A., Cano, M., & Hornero, R. (2021). Abnormal meta-state activation of dynamic brain networks across the Alzheimer spectrum. *NeuroImage*, *232*, 117898. https://doi.org/10.1016/j.neuroimage.2021.117898

Power, J. D., Cohen, A. L., Nelson, S. M., Wig, G. S., Barnes, K. A., Church, J. A., Vogel, A. C., Laumann, T. O., Miezin, F. M., Schlaggar, B. L., & Petersen, S. E. (2011). Functional network organization of the human brain. *Neuron*, *72*(4), 665–678. https://doi.org/10.1016/j.neuron.2011.09.006

Preti, M. G., Bolton, T. A., & Van De Ville, D. (2017). The dynamic functional connectome: State-of-the-art and perspectives. *NeuroImage*, *160*, 41–54. https://doi.org/10.1016/j.neuroimage.2016.12.061

Qu, Y., Wang, P., Liu, B., Song, C., Wang, D., Yang, H., Zhang, Z., Chen, P., Kang, X., Du, K., Yao, H., Zhou, B., Han, T., Zuo, N., Han, Y., Lu, J., Yu, C., Zhang, X., Jiang, T., … Liu, Y. (2021). AI4AD: Artificial intelligence analysis for Alzheimer's disease classification based on a multisite DTI database. *Brain Disorders*, *1*, 100005. https://doi.org/10.1016/j.dscb.2021.100005

Salman, M. S., Du, Y., Lin, D., Fu, Z., Fedorov, A., Damaraju, E., Sui, J., Chen, J., Mayer, A. R., Posse, S., Mathalon, D. H., Ford, J. M., Van Erp, T., & Calhoun, V. D. (2019). Group ICA for identifying biomarkers in schizophrenia: 'Adaptive' networks via spatially constrained ICA show more sensitivity to group differences than spatio-temporal regression. *NeuroImage: Clinical*, *22*, 101747. https://doi.org/10.1016/j.nicl.2019.101747

Scheltens, P., De Strooper, B., Kivipelto, M., Holstege, H., Chetelat, G., Teunissen, C. E., Cummings, J., & van der Flier, W. M. (2021). Alzheimer's disease. *The Lancet*, *397*(10284), 1577–1590. https://doi.org/10.1016/S0140-6736(20)32205-4

Seeley, W. W., Crawford, R. K., Zhou, J., Miller, B. L., & Greicius, M. D. (2009). Neurodegenerative diseases target large-scale human brain networks. *Neuron*, *62*(1), 42–52. https://doi.org/10.1016/j.neuron.2009.03.024

Sendi, M. S. E., Zendehrouh, E., Fu, Z., Liu, J., Du, Y., Mormino, E., Salat, D. H., Calhoun, V. D., & Miller, R. L. (2021). Disrupted dynamic functional network connectivity among cognitive control networks in the progression of Alzheimer's disease. *Brain Connectivity*. Online ahead of print. https://doi.org/10.1089/brain.2020.0847

Sha, Z., van Rooij, D., Anagnostou, E., Arango, C., Auzias, G., Behrmann, M., Bernhardt, B., Bolte, S., Busatto, G. F., Calderoni, S., Calvo, R., Daly, E., Deruelle, C., Duan, M., Duran, F. L. S., Durston, S., Ecker, C., Ehrlich, S., Fair, D., … Francks, C. (2022). Subtly altered topological asymmetry of brain structural covariance networks in autism spectrum disorder across 43 datasets from the ENIGMA consortium. *Molecular Psychiatry*, *27*(4), 2114–2125. https://doi.org/10.1038/s41380-022-01452-7

Tao, Y., Liu, B., Zhang, X., Li, J., Qin, W., Yu, C., & Jiang, T. (2015). The structural connectivity pattern of the default mode network and its association with memory and anxiety. *Frontiers in Neuroanatomy*, *9*, 152. https://doi.org/10.3389/fnana.2015.00152

Wang, J., Zuo, X., Dai, Z., Xia, M., Zhao, Z., Zhao, X., Jia, J., Han, Y., & He, Y. (2013). Disrupted functional brain connectome in individuals at risk for Alzheimer's disease. *Biological Psychiatry*, *73*(5), 472–481. https://doi.org/10.1016/j.biopsych.2012.03.026

Xu, K., Liu, Y., Zhan, Y., Ren, J., & Jiang, T. (2018). BRANT: A versatile and extendable resting-state fMRI toolkit. *Frontiers in Neuroinformatics*, *12*, 52. https://doi.org/10.3389/fninf.2018.00052

Yaesoubi, M., Miller, R. L., & Calhoun, V. D. (2015). Mutually temporally independent connectivity patterns: A new framework to study the dynamics of brain connectivity at rest with application to explain group difference based on gender. *NeuroImage*, *107*, 85–94. https://doi.org/10.1016/j.neuroimage.2014.11.054

Yarkoni, T., Poldrack, R. A., Nichols, T. E., Van Essen, D. C., & Wager, T. D. (2011). Large-scale automated synthesis of human functional neuroimaging data. *Nature Methods*, *8*(8), 665–670. https://doi.org/10.1038/nmeth.1635

Young, A. L., Marinescu, R. V., Oxtoby, N. P., Bocchetta, M., Yong, K., Firth, N. C., Cash, D. M., Thomas, D. L., Dick, K. M., Cardoso, J., van Swieten, J., Borroni, B., Galimberti, D., Masellis, M., Tartaglia, M. C., Rowe, J. B., Graff, C., Tagliavini, F., Frisoni, G. B., … Alzheimer's Disease Neuroimaging Initiative. (2018). Uncovering the heterogeneity and temporal complexity of neurodegenerative diseases with Subtype and Stage Inference. *Nature Communications*, *9*(1), 4273. https://doi.org/10.1038/s41467-018-05892-0

Zhao, K., Zheng, Q., Dyrba, M., Rittman, T., Li, A., Che, T., Chen, P., Sun, Y., Kang, X., Li, Q., Liu, B., Liu, Y., Li, S., & Alzheimer's Disease Neuroimaging Initiative. (2022). Regional radiomics similarity networks reveal distinct subtypes and abnormality patterns in mild cognitive impairment. *Advanced Science*, *9*(12), e2104538. https://doi.org/10.1002/advs.202104538

Zhou, J., & Seeley, W. W. (2014). Network dysfunction in Alzheimer's disease and frontotemporal dementia: Implications for psychiatry. *Biological Psychiatry*, *75*(7), 565–573. https://doi.org/10.1016/j.biopsych.2014.01.020

## SUPPORTING INFORMATION

Additional supporting information can be found online in the Supporting Information section at the end of this article.

**How to cite this article:** Jing, R., Chen, P., Wei, Y., Si, J., Zhou, Y., Wang, D., Song, C., Yang, H., Zhang, Z., Yao, H., Kang, X., Fan, L., Han, T., Qin, W., Zhou, B., Jiang, T., Lu, J., Han, Y., Zhang, X., Liu, B., Yu, C., Wang, P., Liu, Y., & for the Alzheimer's Disease Neuroimaging Initiative (2023). Altered large-scale dynamic connectivity patterns in Alzheimer's disease and mild cognitive impairment patients: A machine learning study. *Human Brain Mapping*, *44*(9), 3467–3480. https://doi.org/10.1002/hbm.26291